Journal of Materials Chemistry C

PAPER

View Article Online
View Journal | View Issue

Cite this: J. Mater. Chem. C, 2017, 5, 848

Effects of a highly lipophilic substituent on the environmental stability of naphthalene tetracarboxylic diimide-based n-channel thin-film transistors†

Liang Zhao,[a] Dongwei Zhang,[b] Yanan Zhu,[b] Sen Peng,[a] Hong Meng*[ab] and Wei Huang[a]

Received 6th October 2016,
Accepted 20th December 2016

DOI: 10.1039/c6tc04323b

www.rsc.org/MaterialsC

N,*N*′-Bis(4-trifluoromethylthiobenzyl)naphthalene-1,4,5,8-tetracarboxylic acid diimide (NTCDI-BSCF$_3$) is synthesized. It shows a similar molecular packing structure and intermolecular transfer integral to *N*,*N*′-bis(4-trifluoromethoxybenzyl)naphthalene-1,4,5,8-tetracarboxylic acid diimide (NTCDI-BOCF$_3$), but demonstrates different behaviors in terms of electron mobility and air stability. NTCDI-BSCF$_3$ based organic thin-film transistors (OTFTs) exhibit much better environmental stability when compared with NTCDI-BOCF$_3$ due to their high hydrophobicity which prevents the diffusion of moisture and oxygen into the devices. In addition, the electron mobility of NTCDI-BSCF$_3$ shows good thermal stability in relation to the deposition temperature, and achieves a value as high as 0.17 cm^2 (V s)$^{-1}$ in air, although it is lower than that of NTCDI-BOCF$_3$. The lower mobility may be attributed to the unexpected crystal growth mode after the deposition of the second monolayer and an insufficient quality of the thin films of NTCDI-BSCF$_3$, especially their inadequate crystallinity. This contrasts with the Stranski–Krastanov (SK) (layer-plus-island) growth mode with the expected crystal growth direction and good crystallinity of NTCDI-BOCF$_3$. Nevertheless, it can be concluded that the introduction of the trifluoromethanesulfenyl (SCF$_3$) group at the N-group of naphthalene tetracarboxylic diimide (NTCDI) is an effective approach for enhancing the environmental stability of NTCDI based n-channel OTFTs.

Introduction

Organic thin-film transistors (OTFTs) have shown great potential as they are essential components for low cost, low energy consumption, large area and flexible organic electronics.[1] Up to now, a great number of p-type,[2–5] n-type[6–8] and ambipolar[9,10] organic semiconductors have been developed. In particular, some p-type organic semiconductors have achieved hole mobilities of greater than 10 cm^2 V^{-1} s^{-1}.[2–4] In contrast, the development of high performance n-type organic semiconductors has been limited by their weaker environmental stability.[11,12] Most of them are sensitive to oxygen and water, which easily cause the device characteristics to vanish after exposure to the ambient air.[13–15] Therefore, the improvement of environmental stability is one of the most important challenges for the development of n-channel organic semiconductors.

Naphthalene tetracarboxylic diimides (NTCDIs) are the most promising n-channel candidates for OTFTs due to their advantages of easy synthesis methods and high electron affinity.[16–18] The environmental stability of OTFTs based on the NTCDI derivatives can be enhanced by introducing electron-withdrawing groups such as fluoroalkyl,[16,19] CN,[20] F[21] and perfluorinated groups[22] to reduce the LUMO level and improve the electron injection at the interface between the organic and electrode layer. In particular, densely packed perfluorinated groups have been demonstrated to provide effective barriers which prevent the diffusion of moisture and oxygen in the active layer,[16,17,23–27] thereby improving the environmental stability of the OTFTs. For example, a CF$_3$ group attached to the NTCDI-benzyl group, instead of a methyl group, significantly enhances the electron mobility by 10^5 times in air,[24] while the replacement of the CF$_3$ group by OCF$_3$ further improves the mobility from 0.12 to 0.7 cm^2 V^{-1} s^{-1}.[28]

[a] Key Laboratory of Flexible Electronics (KLOFE) & Institute of Advanced Materials (IAM), Jiangsu National Synergetic Innovation Center for Advanced Materials (SICAM), Nanjing Tech University (Nanjing Tech), 30 South Puzhu Road, Nanjing, 211816, China. E-mail: iamhmeng@njtech.edu.cn

[b] School of Advanced Materials, Peking University Shenzhen Graduate School, Peking University, Shenzhen, 518055, China

† Electronic supplementary information (ESI) available: Synthesis procedure, ^{1}H NMR and TGA analysis of NTCDI-BSCF$_3$, DSC analysis of NTCDI-BSCF$_3$ and NTCDI-BOCF$_3$, single crystal data, electrochemical and optical properties of NTCDI-BSCF$_3$ and NTCDI-BOCF$_3$, contact angle measurements of pure water on NTCDI-BCF$_3$, NTCDI-BSCF$_3$ and NTCDI-BOCF$_3$ thin films, the hysteresis of NTCDI-BSCF$_3$ based OTFTs, and the analysis of on/off ratios and threshold voltages in relation to time. CCDC 1508499. For ESI and crystallographic data in CIF or other electronic format see DOI: 10.1039/c6tc04323b

With the advantages of the NTCDI core, we aim to develop air stable n-channel organic semiconductors for OTFTs. We know that the trifluoromethanesulfenyl (SCF_3) moiety has higher lipophilicity[29,30] and stronger electron-withdrawing power than the OCF_3 group (see Table S1, ESI†),[31] and is normally applied in the pharmaceutical and agrochemical industries.[32–34] In this study, we intend to introduce the SCF_3 substituent instead of the OCF_3 group in the NTCDI core to enhance the hydrophobicity of the device, which may improve the air stability of n-channel OTFTs. Fortunately, NTCDI-$BSCF_3$ based OTFTs display better environmental stability than that of NTCDI-$BOCF_3$. Interestingly, the two compounds exhibit similar molecular packing structures and intermolecular transfer integrals of their LUMOs, but present significant differences in OTFT characteristics. NTCDI-$BSCF_3$ based OTFTs show excellent thermal stability in electron mobility, which only increases from 0.13 to 0.17 $cm^2\ V^{-1}\ s^{-1}$ as the deposition temperature increases from room temperature (rt) to 70 °C on an octadecyltrichlorosilane (OTS)-treated Si/SiO_2 substrate in ambient air. However, they show lower electron mobility than OTFTs based on NTCDI-$BOCF_3$.[28] The results of the physicochemical properties, X-ray diffraction (XRD), atomic force microscopy (AFM), and crystal growth modes of the thin films are discussed to clarify the effect of substituent variation on the OTFT characteristics.

Experimental section

Synthesis and characterization

The compound NTCDI-$BSCF_3$ was synthesised following the previously reported procedure for synthesizing *N*,*N*′-perfluoroalkyl benzyl NTCDIs.[16] However, instead of using only zinc acetate as a catalyst (as described in the reported procedure), we modified the reaction conditions by combining a small amount of acetic acid with zinc acetate as a synergetic catalyst and reacting 4-(trifluoromethylthio)benzylamine with 1,4,5,8-naphthalene-tetracarboxylic dianhydride in dry DMF to give the high product yield of 83% (Scheme 1). The detailed synthetic procedure is explained in the ESI.† In addition, the chemical structure of NTCDI-$BSCF_3$ was fully confirmed by ^1H NMR, high resolution mass spectrometry (HRMS) and elemental analysis, and the molecular packing structure was also characterized by X-ray crystallography. ^1H NMR (300 Hz, DMSO) δ 8.73 (s, 4H), δ 7.68 (d, J = 6 Hz, 4H), δ 7.58 (d, J = 6 Hz, 4H), δ 5.35 (s, 4H); MALDI-TOF-MS *m*/*z*: 647.99; calcd: 646.58; elemental anal. calcd for $C_{30}H_{16}F_6N_2O_4S_2$: C, 55.73; H, 2.49; N, 4.33; found: C, 55.86; H, 2.61; N, 4.48.

Device fabrication and characterization

The device fabrication procedure and characterization of NTCDI-$BSCF_3$ based OTFTs were done according to the previously reported procedures for fabricating NTCDI-$BOCF_3$ based OTFTs.[28]

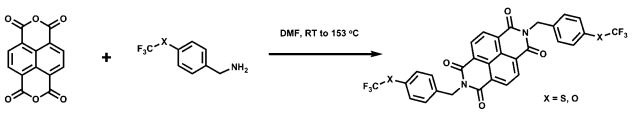

Scheme 1 The synthetic route for NTCDI-$BSCF_3$ and NTCDI-$BOCF_3$.

Results and discussion

Firstly, the physicochemical properties of the two materials were analysed using thermogravimetric analysis (TGA), differential scanning calorimetry (DSC), optical and electrochemical measurements. The TGA results (Fig. S1, ESI†) showed that NTCDI-$BSCF_3$ displays good thermal stability with a decomposition temperature of 376 °C, which is slightly higher than the 352 °C obtained for NTCDI-$BOCF_3$. NTCDI-$BOCF_3$ shows a slightly higher melting point of 316 °C than that of NTCDI-$BSCF_3$ (300 °C) (Fig. S2, ESI†). In addition, the optical and electrochemical properties of NTCDI-$BSCF_3$ were evaluated in thin film and dichloromethane solution (Fig. 1). The comparison between the two materials is summarized in Table S3 (ESI†). The results of UV-vis absorption spectra show that NTCDI-$BSCF_3$ has a slight hypochromic shift compared with NTCDI-$BOCF_3$. However, an energy bandgap of approximately 3 eV is obtained for both of the materials. For the cyclic voltammetry (CV) analysis, NTCDI-$BSCF_3$ was thermally evaporated on a glass carbon electrode (GCE) for measurements based on the calibration of redox potentials of an internal ferrocene reference (F_c/F_c^+). The LUMO energy level of NTCDI-$BSCF_3$ (*ca.* −4.03 eV below the vacuum level) is slightly higher, by about 0.2 eV, than that of NTCDI-$BOCF_3$, as judged from the cathodic shift of the reduction potential in the CV measurements (Fig. 1b). Generally, the LUMO energy level of n-channel semiconductors should be less than or equal to −4.0 eV for ambient stable electron transport and injection in n-channel OTFTs.[35–38] Obviously, NTCDI-$BSCF_3$ is promising as an air stable n-channel semiconductor.

We wanted to reach a preliminary understanding of the effect of the SCF_3 group, instead of the OCF_3 substituent in the NTCDI core, on the electron transfer properties. Therefore the intermolecular transfer integrals of the LUMO were firstly analysed by importing the single crystal data into the Amsterdam density functional (ADF) simulation software,[39] which was operated with the basis set of triple-Z 2 plus polarization function (TZ2P) and with the PW91 functional (GGA:PW91) for the calculations. The molecular packing structure of NTCDI-$BSCF_3$ was obtained from the single crystal which was grown by the vapor transport process and analysed by X-ray crystallography. The detailed molecular packing structure and intermolecular transfer integral of NTCDI-$BSCF_3$ are shown in Fig. 2. As can be seen, NTCDI-$BSCF_3$ shows a herringbone-like molecular packing structure with a dihedral angle of 95° (Fig. 2a). The interplanar distances in the *a*, *b* and *c* axes directions are

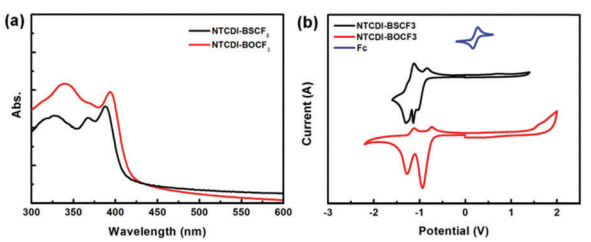

Fig. 1 UV-vis (a) and CV (b) measurements of NTCDI-$BSCF_3$ evaluated in thin film and dichloromethane solution, respectively.

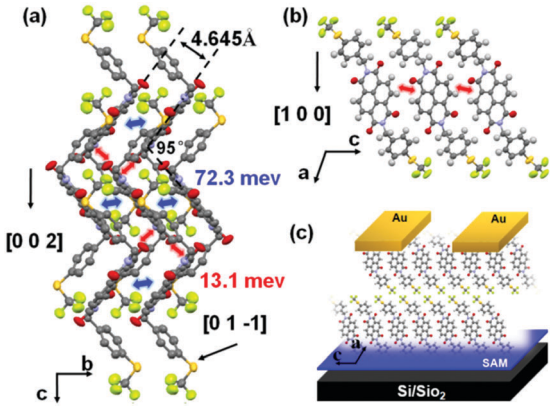

Fig. 2 The molecular packing structures of (a) bc and (b) ac planes and related intermolecular transfer integrals of the LUMO for NTCDI-BSCF$_3$; (c) The molecular arrangement of NTCDI-BSCF$_3$ on OTS treated Si/SiO$_2$ substrate.

found to be 20.943, 4.645 and 14.264 Å, respectively. These results are almost identical to those for NTCDI-BOCF$_3$ (Table S2, ESI†), implying that the two compounds may have similar electron transfer properties. As expected, the transfer integrals of the LUMO in the strong face-to-face intermolecular interactions and in the opposite direction of neighboring molecules are calculated to be 72.3 and 13.1 meV (Fig. 2a and b), respectively, for NTCDI-BSCF$_3$, which are slightly lower than the values of 79.7 and 14.1 meV obtained for NTCDI-BOCF$_3$. In general, larger intermolecular orbital overlaps provide better electron transport properties in OTFTs,[40] predicting that NTCDI-BOCF$_3$ may exhibit better electrical performance than NTCDI-BSCF$_3$.

Interestingly, NTCDI-BSCF$_3$ and NTCDI-BOCF$_3$ have similar molecular packing structures and close intermolecular transfer integrals of their LUMOs, but they show significant differences in OTFT device characteristics. The typical reverse transfer and output characteristics of NTCDI-BSCF$_3$ based OTFTs are shown in Fig. 3, and the related hysteresis for I_d are provided in Fig. S3 (ESI†). The related device characteristics are summarised in Table 1. As can be seen, the electron mobility of NTCDI-BSCF$_3$ is only 0.026 cm^2 V^{-1} s^{-1} on the UV-treated substrate, but is enhanced to 0.08 and 0.13 cm^2 V^{-1} s^{-1} after F-SAM and OTS treatment, respectively. In addition, NTCDI-BSCF$_3$ based OTFTs show good thermal stability in relation to the deposition temperature. The electron mobility is maintained at 0.17 cm^2 V^{-1} s^{-1} after increasing the deposition temperature to 70 °C on the OTS-treated substrate. Moreover, the results are consistent with the previous predictions, and the electron mobility of NTCDI-BSCF$_3$ is much lower than that of the NTCDI-BOCF$_3$ (0.7 cm^2 V^{-1} s^{-1}) obtained at the same deposition temperature.[28]

A contrastive XRD analysis of NTCDI-BSCF$_3$ and NTCDI-BOCF$_3$ thin films was done to further understand the effect of side chain replacement on the device performance, as shown in Fig. 4a. As expected, the two compounds show the Sharp Bragg's reflections up to the fifth order at very similar positions due to their similar molecular packing structures. The diffraction peaks of NTCDI-BSCF$_3$ at 2θ = 4.59°, 8.93°, 13.24°, 17.72° and 26.72° correspond to the diffractions of (100), (200), (300), (400) and (600) planes, respectively. Thereby, a d spacing distance (d_{100}) of 1.93 nm is obtained, which is nearly the same as the value of 1.95 nm obtained for NTCDI-BOCF$_3$. This investigation implies that NTCDI-BSCF$_3$ molecules should exhibit a similar stacking pattern to NTCDI-BOCF$_3$, which is almost aligned vertically on the OTS-treated substrate. However, the intensity of each peak shows a slight enhancement when the deposition temperature is increased from rt to 70 °C for NTCDI-BSCF$_3$, indicating that the deposition temperature only exerts a trivial effect on the crystalline quality of the thin films. The results are consistent with the thermal stability of the mobility of OTFTs in relation to the deposition temperature (see Table 1). In contrast, NTCDI-BOCF$_3$ exhibits stronger intensity diffraction peaks with a massive dependence on the deposition temperature when compared with NTCDI-BSCF$_3$, implying the better crystallinity of the NTCDI-BOCF$_3$ thin film that results in the higher performance of its OTFTs.

The temperature-dependent thin-film morphology of NTCDI-BSCF$_3$ was analysed by AFM, as shown in Fig. 4b and c. Rod like grains become larger as the deposition temperature increases to 70 °C in the thin films of NTCDI-BSCF$_3$, which is similar to

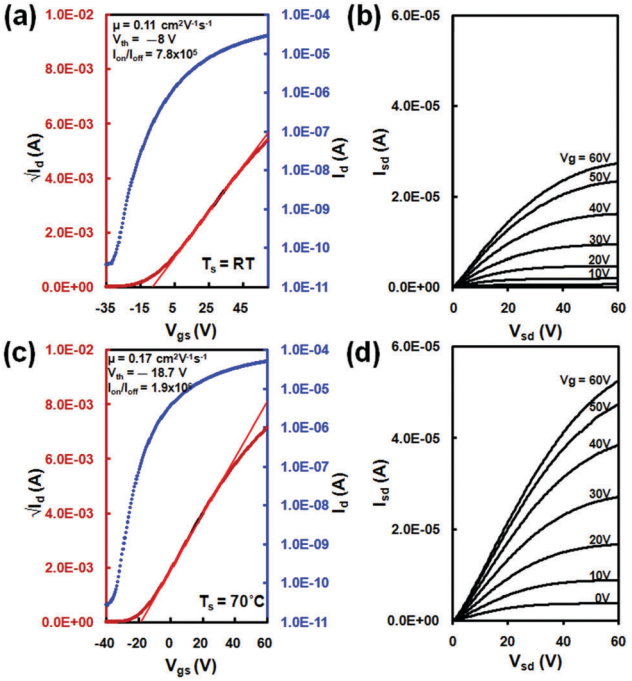

Fig. 3 Typical transfer and output curves of NTCDI-BSCF$_3$ based OTFTs deposited at rt (a and b) and 70 °C (c and d) on an OTS-treated Si/SiO$_2$ substrate.

Table 1 Device performance of NTCDI-BSCF$_3$

Polycrystalline thin-film device					
SAM	T_{sub} (°C)	Av. mobility (cm^2 V^{-1} s^{-1})	Max. mobility (cm^2 V^{-1} s^{-1})	I_{on}/I_{off}	V_{th} (V)
OTS	RT	0.11 ± 0.01	0.13	8.86 × 10^5	−5.6
OTS	70	0.16 ± 0.01	0.17	1.76 × 10^6	−20.1
F-SAM	RT	0.079 ± 0.006	0.085	5.37 × 10^5	9.7
Bare	RT	0.024 ± 0.002	0.026	4.10 × 10^4	9.3

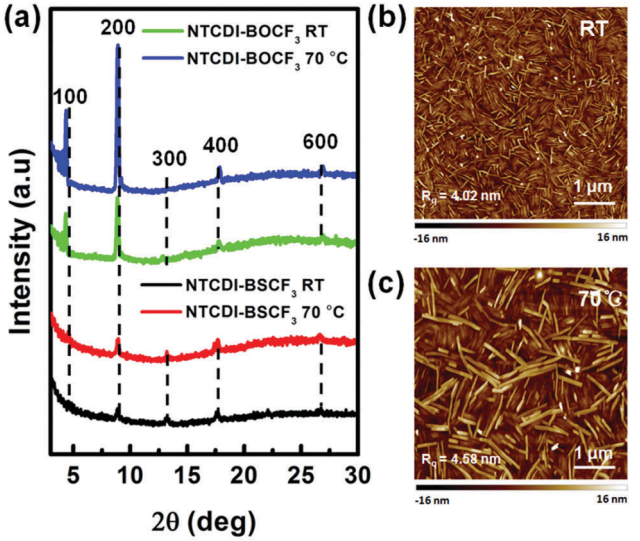

Fig. 4 NTCDI-BSCF$_3$ thin films deposited at rt and 70 °C on the OTS-treated Si/SiO$_2$ substrates: (a) comparison of X-ray diffractions between NTCDI-BSCF$_3$ and NTCDI-BOCF$_3$ thin films; AFM morphology (2 × 2 μm^2) of NTCDI-BSCF$_3$ thin films deposited at (b) rt and (c) 70 °C.

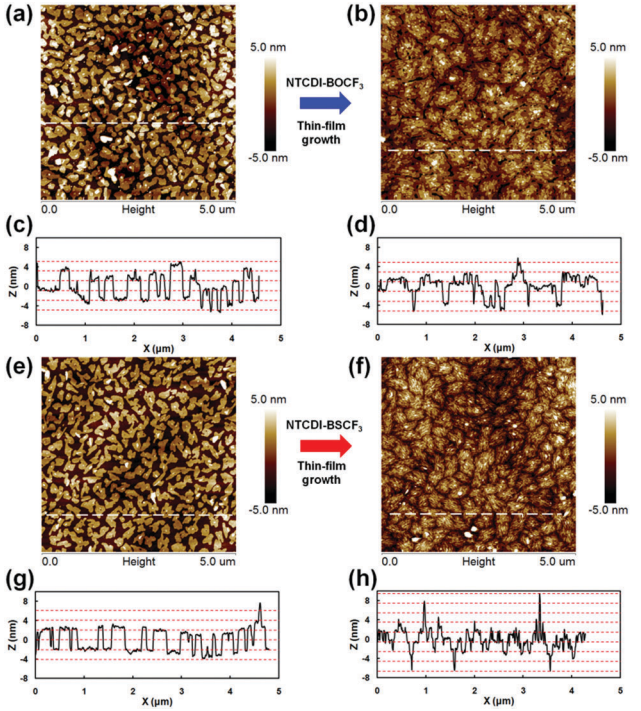

Fig. 5 AFM images (5 × 5 μm^2) of NTCDI-BOCF$_3$ and NTCDI-BSCF$_3$ thin films deposited at rt with increasing thickness on the OTS treated Si/SiO$_2$ substrates. The initial layer of NTCDI-BOCF$_3$ (a) and NTCDI-BSCF$_3$ (e) thin films and their corresponding line scans (c and g) obtained from AFM measurements along the white dashed lines in parts (a) and (e). The continuous growth of NTCDI-BOCF$_3$ (b) and NTCDI-BSCF$_3$ (f) thin films and their corresponding line scans (d and h) obtained from AFM measurements along the white dashed lines in parts (b) and (f).

the morphology seen for NTCDI-BOCF$_3$. In general, larger gain sizes provide a positive effect on device performance,[26,41–43] indicating that a higher mobility should be achieved at a substrate temperature of 70 °C. However, the mobility enhancement was almost negligible in the case of NTCDI-BSCF$_3$, significantly differing from that for NTCDI-BOCF$_3$. To further understand the mobility difference between NTCDI-BSCF$_3$ and NTCDI-BOCF$_3$, a thin-film structural analysis of both materials was investigated by continuously introducing two and four monolayers (ML) with nominal thicknesses on the OTS treated Si/SiO$_2$ substrates as shown in Fig. 5a–h. Based on the AFM images of Fig. 5a and e, Stranski–Krastanov (SK) mode[44] (layer-plus-island) growth was proven for the film deposition processes of both materials. From the analysis of the corresponding line scans (Fig. 5c and g), the average step height of the island was obtained as ∼4 nm, which is approximately equal to the height of two monolayers. After consecutively growing a nominal thickness of 4 ML, the thin-film growths of the two materials exhibit significantly different behaviors. For the NTCDI-BOCF$_3$ thin film (Fig. 5b), deposition tends to occur for the first two layers in a horizontal direction, and the third and fourth layers also gradually grow on the grain island (Fig. 5d). In contrast, the NTCDI-BSCF$_3$ thin film (Fig. 5f) tends to grow in the vertical direction and the third, fourth and even seventh monolayers nucleate and grow on the grain island (see Fig. 5h). By comparing 4 ML AFM images of these two materials, we can establish that the grain size of the NTCDI-BOCF$_3$ thin film is obviously larger than that of NTCDI-BSCF$_3$, especially for the first two layers. Based on this investigation of crystal growth mode, we can predict that the grains of NTCDI-BOCF$_3$ thin film will be gradually connected together such that voids in the grain boundary vanish and the film becomes a unity for the initial few monolayers. However, the grain boundary voids of the NTCDI-BSCF$_3$ thin film may not vanish easily due to the unexpected thin-film growth direction. In general, better continuity of thin film always provides better carrier mobility. Based on the AFM and XRD analysis, it can be concluded that the electron mobility of NTCDI-BSCF$_3$ should be lower than that of NTCDI-BOCF$_3$ due to the difference in the crystal growth mode and its poor thin-film crystallinity.

As mentioned earlier, both compounds are promising candidates for air stable n-channel OTFTs due to their suitable LUMO energy levels and the protection from oxygen and moisture of the perfluorinated groups on the molecular center. To further understand the effect of substituent replacement on the environmental stability of the devices, the previously reported NTCDI-BCF$_3$ has been synthesized and compared with the above two compounds. Five of each of the NTCDI-BSCF$_3$, NTCDI-BOCF$_3$ and NTCDI-BCF$_3$ based OTFTs were exposed in ambient air with a high humidity of around 45 to 80% for 15 days. The related degradation rates of the average device performances are shown in Fig. 6. As can be seen, the electron mobilities of these three compounds show a decreasing trend in relation to time. Similar degradation rates are obtained for NTCDI-BCF$_3$ and NTCDI-BOCF$_3$ based OTFTs, which are degraded by 42% and 40%, respectively, within 15 days. These rates are obviously faster than that of NTCDI-BSCF$_3$ which degraded by 33%. This directly indicates the better environmental stability of NTCDI-BSCF$_3$ based OTFTs than of NTCDI-BCF$_3$ and

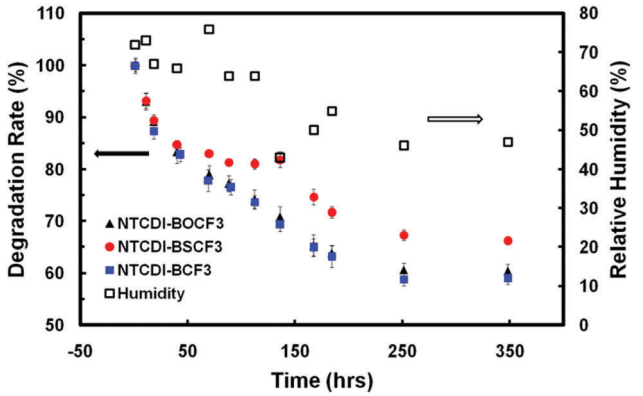

Fig. 6 The electron-mobility degradation rate for the NTCDI-$BSCF_3$, NTCDI-$BOCF_3$ and NTCDI-BCF_3 based OTFTs, and the relative humidity in ambient air.

NTCDI-$BOCF_3$ based OTFTs. As we know, hydrophobicity and closely packed perfluorinated groups have been demonstrated to protect the thin films from oxygen and moisture,[16,26,27] thereby enhancing the stability of the device performance in ambient air. In this case, the shortest interplane distance of NTCDI-BCF_3 is slightly larger than that of NTCDI-$BSCF_3$ and NTCDI-$BOCF_3$ (see Table S2, ESI†), implying the worst environmental stability of NTCDI-BCF_3. However, NTCDI-$BSCF_3$ and NTCDI-$BOCF_3$ exhibited similar molecular packing structure, implying that the hydrophobicity of the thin films could be the major factor leading to the enhancement of the environmental stability of the NTCDI-$BSCF_3$ device. In order to clarify the reason, contact angle measurements were investigated by placing 1 μL of pure water on the NTCDI-$BOCF_3$, NTCDI-$BSCF_3$ and NTCDI-BCF_3 thin films, and results are shown in Fig. S4 (ESI†). As predicted, the contact angle on the NTCDI-BSCF3 thin films (111°) is found to be larger than those on the NTCDI-$BOCF_3$ thin films (104°) and NTCDI-BCF_3 thin films (103°) due to the higher lipophilicity of the SCF_3 substituent than of the OCF_3 and CF_3 groups. Based on the high hydrophobicity of the thin films, NTCDI-$BOCF_3$ and NTCDI-BCF_3 based OTFTs should exhibit similar environmental stability, which is lower than that of NTCDI-$BSCF_3$. This matched well with the results of the environmental stability tests of these three compounds. In addition, the variations of the related threshold voltages and on/off ratios of the three compound based OTFTs in relation to time are shown in Fig. S5 (ESI†). NTCDI-$BSCF_3$ shows the lowest on/off ratio in comparison to NTCDI-$BOCF_3$ and NTCDI-BCF_3 due to its lower on-current in air. The on/off ratios of these three compounds gradually degrade within 15 days due to the degradation of the on-current. Moreover, the threshold voltages are gradually increased with storage time.

The highly lipophilic and electron-withdrawing SCF_3 group is a typical moiety in the family of fluorine-containing substituents.[45] The modification of NTCDIs by replacing the OCF_3 substituent with the SCF_3 moiety enhances the hydrophobicity of the thin films to prevent the diffusion of moisture and oxygen, thereby greatly improving the environmental stability of NTCDI-based n-channel OTFTs. In contrast, the mobility decay is still significantly larger than that found for other n-type organic molecules,[16,21,46] *e.g.* the electrical property of PTCDI-C_4F_7[21] can be maintained for 60 days without obvious degradation. This is because PTCDI-C_4F_7 has a denser molecular packing structure with the shortest interplane distance of only 3.31 Å, which is much lower than those of NTCDI-$BSCF_3$ and NTCDI-$BOCF_3$ (4.645 and 4.649 Å, respectively). In addition, the introduction of the highly lipophilic electron-withdrawing SCF_3 group to replace the OCF_3 group only slightly changes the molecular packing structure and the intermolecular transfer integral, indicating similar carrier transport properties for the two compounds. Unfortunately, the SCF_3 group caused a negative effect on the thin-film quality and growth mode, especially on the crystallinity, which is likely to be the major factor causing the reduction of the device performance. The crystallinity of NTCDI-$BOCF_3$ thin films is found to be enhanced by increasing the deposition temperature. In contrast, the enhancement of the crystallinity is negligible for NTCDI-$BSCF_3$ (see Fig. 4a), directly showing its poor crystallinity, and leading to the inefficient electron transport in NTCDI-$BSCF_3$ based OTFTs. Based on the above investigations, it can be concluded that the introduction of a highly lipophilic electron-withdrawing group (*e.g.* SCF_3 group) is an effective approach for the improvement of air stable n-channel OTFTs. A dense molecular packing structure with better thin-film crystallinity and a highly lipophilic group could provide a new impetus for the development of high performance environmentally stable n-type organic semiconductors.

Conclusions

In this study, NTCDI-$BSCF_3$ was synthesized and systematically compared with NTCDI-$BOCF_3$. The environmental stability of NTCDI based n-channel OTFTs was found to be significantly enhanced by the replacement of the electron-withdrawing OCF_3 group with the highly lipophilic SCF_3 substituent in the NTCDI core. In addition, the SCF_3 substituent only slightly changed the molecular packing structure and the intermolecular transfer integral of the LUMO, but greatly affected the OTFT device performance. In contrast to the high performance of NTCDI-$BOCF_3$, NTCDI-$BSCF_3$ thin films showed poor crystallinity and an SK growth mode with an unexpected crystal growth direction after the deposition of the second monolayer. However, NTCDI-$BSCF_3$ based OTFTs showed good thermal stability in relation to the deposition temperature, and achieved an electron mobility of 0.17 $cm^2 V^{-1} s^{-1}$ at the deposition temperature of 70 °C on an OTS-treated Si/SiO_2 substrate. Although the mobility of NTCDI-$BSCF_3$ is insufficient, the SCF_3 group with its higher lipophilicity and strong electron-withdrawing behavior has been demonstrated as a suitable substituent for the molecular design of air stable n-channel semiconductors. It has great potential in the development of high performance environmentally stable n-channel OTFTs if the molecular packing structure and the crystallinity can be regulated in the molecular design.

Acknowledgements

The work was supported by NSFC (51373075), the National Research Foundation for the Doctoral Program (20133221110004), the

National Basic Research Program of China (973 Program, No. 2015CB856500; 2015CB932200), Shenzhen Key Laboratory of Shenzhen Science and Technology Plan (ZDSYS20140509094114164), Guangdong Key Research Project (2015B090914002; 2014B090914003), Guangdong Talents Project, Guangdong Academician Workstation (2013B090400016) and the Natural Science Foundation of Guangdong Province (2014A030313800).

References

1 S. R. Forrest, *Nature*, 2004, **428**, 911–918.
2 Y. Diao, B. C. K. Tee, G. Giri, J. Xu, D. H. Kim, H. A. Becerril, R. M. Stoltenberg, T. H. Lee, G. Xue, S. C. B. Mannsfeld and Z. Bao, *Nat. Mater.*, 2013, **12**, 665–671.
3 H. Iino, T. Usui and J.-I. Hanna, *Nat. Commun.*, 2015, **6**, 6828.
4 H. Minemawari, T. Yamada, H. Matsui, J. Y. Tsutsumi, S. Haas, R. Chiba, R. Kumai and T. Hasegawa, *Nature*, 2011, **475**, 364–367.
5 X. Gao and Z. Zhao, *Sci. China: Chem.*, 2015, **58**, 947–968.
6 H. Luo, Z. Cai, L. Tan, Y. Guo, G. Yang, Z. Liu, G. Zhang, D. Zhang, W. Xu and Y. Liu, *J. Mater. Chem. C*, 2013, **1**, 2688–2695.
7 D. Shukla, S. F. Nelson, D. C. Freeman, M. Rajeswaran, W. G. Ahearn, D. M. Meyer and J. T. Carey, *Chem. Mater.*, 2008, **20**, 7486–7491.
8 F. Zhang, Y. Hu, T. Schuettfort, C.-A. Di, X. Gao, C. R. McNeill, L. Thomsen, S. C. B. Mannsfeld, W. Yuan, H. Sirringhaus and D. Zhu, *J. Am. Chem. Soc.*, 2013, **135**, 2338–2349.
9 L. Ren, C. Liu, Z. Wang and X. Zhu, *J. Mater. Chem. C*, 2016, **4**, 5202–5206.
10 O. Pitayatanakul, T. Higashino, T. Kadoya, M. Tanaka, H. Kojima, M. Ashizawa, T. Kawamoto, H. Matsumoto, K. Ishikawa and T. Mori, *J. Mater. Chem. C*, 2014, **2**, 9311–9317.
11 J. E. Anthony, A. Facchetti, M. Heeney, S. R. Marder and X. Zhan, *Adv. Mater.*, 2010, **22**, 3876–3892.
12 C. Wang, H. Dong, W. Hu, Y. Liu and D. Zhu, *Chem. Rev.*, 2012, **112**, 2208–2267.
13 B. A. Jones, A. Facchetti, M. R. Wasielewski and T. J. Marks, *J. Am. Chem. Soc.*, 2007, **129**, 15259–15278.
14 S. Nagamatsu, S. Oku, K. Kuramoto, T. Moriguchi, W. Takashima, T. Okauchi and S. Hayase, *ACS Appl. Mater. Interfaces*, 2014, **6**, 3847–3852.
15 X. Chen, Y. Guo, L. Tan, G. Yang, Y. Li, G. Zhang, Z. Liu, W. Xu and D. Zhang, *J. Mater. Chem. C*, 2013, **1**, 1087–1092.
16 H. E. Katz, A. J. Lovinger, J. Johnson, C. Kloc, T. Siegrist, W. Li, Y. Y. Lin and A. Dodabalapur, *Nature*, 2000, **404**, 478–481.
17 J. H. Oh, S. Liu, Z. Bao, R. Schmidt and F. Würthner, *Appl. Phys. Lett.*, 2007, **91**, 212107.
18 X. Gao, C.-a. Di, Y. Hu, X. Yang, H. Fan, F. Zhang, Y. Liu, H. Li and D. Zhu, *J. Am. Chem. Soc.*, 2010, **132**, 3697–3699.
19 A. Facchetti, M. Mushrush, H. E. Katz and T. J. Marks, *Adv. Mater.*, 2003, **15**, 33–38.
20 B. A. Jones, M. J. Ahrens, M.-H. Yoon, A. Facchetti, T. J. Marks and M. R. Wasielewski, *Angew. Chem., Int. Ed.*, 2004, **43**, 6363–6366.
21 R. Schmidt, J. H. Oh, Y.-S. Sun, M. Deppisch, A.-M. Krause, K. Radacki, H. Braunschweig, M. Könemann, P. Erk, Z. Bao and F. Würthner, *J. Am. Chem. Soc.*, 2009, **131**, 6215–6228.
22 M.-H. Yoon, A. Facchetti, C. E. Stern and T. J. Marks, *J. Am. Chem. Soc.*, 2006, **128**, 5792–5801.
23 H. E. Katz, Z. Bao and S. L. Gilat, *Acc. Chem. Res.*, 2001, **34**, 359–369.
24 H. E. Katz, J. Johnson, A. J. Lovinger and W. Li, *J. Am. Chem. Soc.*, 2000, **122**, 7787–7792.
25 C.-C. Kao, P. Lin, C.-C. Lee, Y.-K. Wang, J.-C. Ho and Y.-Y. Shen, *Appl. Phys. Lett.*, 2007, **90**, 212101.
26 J. H. Oh, S. L. Suraru, W.-Y. Lee, M. Könemann, H. W. Höffken, C. Röger, R. Schmidt, Y. Chung, W.-C. Chen, F. Würthner and Z. Bao, *Adv. Funct. Mater.*, 2010, **20**, 2148–2156.
27 B. Kang, R. Kim, S. B. Lee, S.-K. Kwon, Y.-H. Kim and K. Cho, *J. Am. Chem. Soc.*, 2016, **138**, 3679–3686.
28 D. Zhang, L. Zhao, Y. Zhu, A. Li, C. He, H. Yu, Y. He, C. Yan, O. Goto and H. Meng, *ACS Appl. Mater. Interfaces*, 2016, **8**, 18277–18283.
29 F. R. Leroux, B. Manteau, J.-P. Vors and S. Pazenok, *Beilstein J. Org. Chem.*, 2008, **4**, 13.
30 T. Bootwicha, X. Liu, R. Pluta, I. Atodiresei and M. Rueping, *Angew. Chem., Int. Ed.*, 2013, **52**, 12856–12859.
31 C. Hansch, A. Leo and R. W. Taft, *Chem. Rev.*, 1991, **91**, 165–195.
32 T. Liang, C. N. Neumann and T. Ritter, *Angew. Chem., Int. Ed.*, 2013, **52**, 8214–8264.
33 C. Xu, B. Ma and Q. Shen, *Angew. Chem., Int. Ed.*, 2014, **53**, 9316–9320.
34 X.-H. Xu, K. Matsuzaki and N. Shibata, *Chem. Rev.*, 2015, **115**, 731–764.
35 X. Gao and Y. Hu, *J. Mater. Chem. C*, 2014, **2**, 3099–3117.
36 Z. Wang, C. Kim, A. Facchetti and T. J. Marks, *J. Am. Chem. Soc.*, 2007, **129**, 13362–13363.
37 H. Usta, A. Facchetti and T. J. Marks, *Acc. Chem. Res.*, 2011, **44**, 501–510.
38 H. Usta, C. Risko, Z. Wang, H. Huang, M. K. Deliomeroglu, A. Zhukhovitskiy, A. Facchetti and T. J. Marks, *J. Am. Chem. Soc.*, 2009, **131**, 5586–5608.
39 G. te Velde, F. M. Bickelhaupt, E. J. Baerends, C. Fonseca Guerra, S. J. A. van Gisbergen, J. G. Snijders and T. Ziegler, *J. Comput. Chem.*, 2001, **22**, 931–967.
40 M. Nakano, I. Osaka, D. Hashizume and K. Takimiya, *Chem. Mater.*, 2015, **27**, 6418–6425.
41 Q. Wu, X. Qiao, Q. Huang, J. Li, Y. Xiong, X. Gao and H. Li, *RSC Adv.*, 2014, **4**, 16939–16943.
42 D. Raoufi, A. Kiasatpour, H. R. Fallah and A. S. H. Rozatian, *Appl. Surf. Sci.*, 2007, **253**, 9085–9090.
43 B. J. Jung, J. Sun, T. Lee, A. Sarjeant and H. E. Katz, *Chem. Mater.*, 2009, **21**, 94–101.
44 J. A. Venables, G. D. T. Spiller and M. Hanbucken, *Rep. Prog. Phys.*, 1984, **47**, 399.
45 Y. Yang, L. Xu, S. Yu, X. Liu, Y. Zhang and D. A. Vicic, *Chem. – Eur. J.*, 2016, **22**, 858–863.
46 H. Z. Chen, M. M. Ling, X. Mo, M. M. Shi, M. Wang and Z. Bao, *Chem. Mater.*, 2007, **19**, 816–824.